

26. W. Harrison, D. Elsberg, K. Echelmeyer, R. Krimmel, *J. Glaciol.* **47**, 659 (2002).
 27. S. M. Hodge *et al.*, *J. Clim.* **11**, 2161 (1998).
 28. M. S. Pelto, M. M. Miller, *Northwest Sci.* **64**, 121 (1990).
 29. M. M. Miller, M. S. Pelto, *Geogr. Ann.* **81A**, 671 (1999).
 30. Supported by grants from NSF (Arctic Natural Sci-

ences, OPP-987-6421), NOAA (Climate Change Detection and Attribution Project, NA86GP0470), and NASA (Cryospheric Sciences, NAGW-3727). J. Mitchell, K. Abnett, G. Adalgeirsdóttir, P. Del Vecchio, D. Elsberg, T. J. Fudge, C. Larsen, H. Li, R. Muskett, A. Post, B. Rabus, J. Sapiano, W. Seider, L. Sornbardier, and S. Zirnheld assisted with the project.

Supporting Online Material

www.sciencemag.org/cgi/content/full/297/5580/382/DC1

Supporting Text

Figs. S1 and S2

Table S1

3 April 2002; accepted 5 June 2002

Freshening of the Ross Sea During the Late 20th Century

S. S. Jacobs,* C. F. Giulivi, P. A. Mele

Ocean measurements in the Ross Sea over the past four decades, one of the longest records near Antarctica, reveal marked decreases in shelf water salinity and the surface salinity within the Ross Gyre. These changes have been accompanied by atmospheric warming on Ross Island, ocean warming at depths of ~300 meters north of the continental shelf, a more negative Southern Oscillation Index, and thinning of southeast Pacific ice shelves. The freshening appears to have resulted from a combination of factors, including increased precipitation, reduced sea ice production, and increased melting of the West Antarctic Ice Sheet.

General circulation models of a moderately warmer climate typically show larger changes at high latitudes, such as increased precipitation and ice sheet growth, a reduced but possibly thicker sea ice cover, and weaker deep ocean convection (1, 2). A freshening of 0.001 per year (a^{-1}) in Antarctic intermediate water (AAIW) in the South Pacific over ~25 years, coincident with a salinity increase at shallower depths, has been attributed mainly to an intensification of the atmospheric hydrological cycle (3). That salinity decrease implies a large increase in the freshwater flux at high southern latitudes where intermediate water is formed. Changes in precipitation minus evaporation may be inferred from mixed layer salinity, but near-surface salinity variability is high in regions where sea ice forms and melts every year. The production of sea ice adds brine to waters over the continental shelf, and its northward export and melting lowers the salinity of the upper ocean between the shelf and Polar Front. A slower stage of the hydrological cycle returns fresh water to the ocean by the melting of ice shelves and icebergs. Climatic perturbations of these processes and of the upwelling rate of deep water can alter the salinity of waters that originate in the Southern Ocean.

In the Pacific sector of the Southern Ocean, sea ice formation and export is strongest in the southwest Ross Sea (Fig. 1), where persistent winter polynyas are located near the Ross Ice Shelf and Victoria Land coast (4, 5). A substantial decrease in shelf water salinity has occurred

in that region over the past four decades (Fig. 2), extending eastward near the ice front (Fig. 3A) and throughout the western continental shelf (6). Formed at the sea surface in winter, the shelf water is vertically stabilized by salinities that increase with depth, but the entire water mass has shifted toward lower values since the 1960s. Although the saltiest water in the Southern Ocean has historically been found in the southwest Ross Sea, this lengthy decline has relocated that maximum to the Weddell Sea (7).

Sea ice production over the Antarctic continental shelf depends mainly on wind strength, air temperature, and shelf area. Lengthy wind measurements are lacking, but temperatures have risen ~1.0°C on Ross Island since 1957 (6). That is ~5% of the difference between the -20°C annual mean and the sea surface freezing point, which may thus account for a small fraction of the observed salt deficit. A concurrent northward advance of the Ross Ice Shelf covered ~6% of the open shelf region where sea ice can form, but any resulting decrease in sea ice production may have been partly compensated by more marine ice growth beneath a larger ice shelf (8).

The volume of sea ice exported from the continental shelf can be roughly estimated from ice thickness measurements (9) and mean National Centers for Environmental Prediction surface winds of ~6 m s^{-1} in the northwest sector since 1985 (10). This export is equivalent to a mean thickness of $2.5 \pm 0.8 \text{ m a}^{-1}$ over 9 months and a 400,000 km^2 shelf area, assuming a 10% uncertainty in ice and wind measurements and exit gate width. For comparison, shelf water freshening that resulted entirely from reduced sea ice production would require

an export decline of ~3.1 m in recent decades. This seems unrealistic, because it would imply a large and undocumented reduction in wind strength, which in turn could result in thicker ice and a slower ocean circulation, with the latter likely to increase shelf water residence time and salinity.

A major decrease in sea ice production also appears inconsistent with reported increases in ice extent, ice concentration, and length of the sea ice season in the Ross Sea since 1978 (11, 12). Those changes depend mainly on areas north of the continental shelf, however, and could mask a thinner ice cover resulting from changes in surface forcing. East of the Ross Sea, a larger atmospheric warming trend and substantial declines in sea ice extent and season have been documented over recent decades (12, 13). Most of that sea ice change has occurred above the eastward-flowing Antarctic Circumpolar Current, but if the regional warming in that sector reduced ice production further south, it would have lowered the salinity of the westward coastal current.

The salinity of shelf water in the Ross Sea is less influenced by precipitation and local ice shelf melting than by sea ice export. For 8 to 9 months each year, most precipitation will also fall on sea ice that is advected off the continental shelf. Where that precipitation is sufficient to sink the ice freeboard, snow-induced sea ice production and brine drainage would cause a salinity increase in the water column. Net melting as high as 25 cm a^{-1} beneath the ~500,000- km^2 Ross Ice Shelf (14) would compensate for <20% of the brine derived from the sea ice cycle. Moreover, modeling sensitivity studies indicate that ice shelf melting would decrease in response to a weaker thermohaline circulation associated with lower salinity (15). Plausible changes in local precipitation and glacial ice melting therefore cannot explain the large decline in shelf water salinity.

The only other important sources of freshening for the Ross Sea continental shelf are waters imported by the coastal current and waters along the southern edge of the Ross Gyre. Evaluating salinity changes in these surface waters encounters problems of high spatial and temporal variability, along with sparse historical ocean measurements east of the Ross Sea. As an alternative, we have focused on salinity at the temperature minimum (T_{min}) within the Ross Gyre. The T_{min} is a well-defined subsurface feature in most off-

Lamont-Doherty Earth Observatory of Columbia University, Palisades, NY 10964, USA.

*To whom correspondence should be addressed. E-mail: sjacobs@ldeo.columbia.edu

REPORTS

shelf summer data, occurring at a mean depth of ~65 m in this region and represented in winter by mixed layer salinities. An edited database for the interior Ross Gyre is reasonably well distributed over the study area (Fig. 1) and was divided into several subregions to assess the spatial and temporal variability. A T_{min} salinity decrease occurs in all areas and is strongest in the southern and eastern sectors (Fig. 3B). The average gyre salinity decline is twice that in the deeper water column on the continental shelf, strongly pointing to an external origin for much of the shelf water salinity decrease. Evidently, the Ross Sea continental shelf has recently been importing fresher and/or more surface water relative to the inflow of modified circumpolar deep water (MCDW) (16).

The Ross Gyre surface water salinity change is equivalent to a freshwater increase of 18 mm a^{-1} to a depth of 100 m, or 72 cm over 4 decades. That is a rather large change as compared to the 10 to 40 cm a^{-1} climatological European Center for Medium-Range Weather Forecasts mean for this sector or to modeled increases resulting from atmospheric warming at these latitudes (1). Similarly, the change is large compared to a 2.4 mm a^{-1} increase in the 15.1 cm a^{-1} annual mean over Antarctica (17). The increase is smaller than the 31 mm a^{-1} estimated to account for South Pacific AAIW

freshening (3), but that value could have been substantially higher or lower with different source area assumptions. Increased precipitation could result from multidecadal Southern Oscillation variability, given its strong links to the Bellingshausen, Amundsen, and Ross Seas, and the correlation between its more negative index and increased precipitation on Antarctica (17, 18).

The upstream melting of ice shelves and icebergs also influences the salinity of Ross Gyre and coastal waters. The observed decrease in shelf water salinity is equivalent to adding 6.5 cm more fresh water each year to a 750-m water column. The observed salinity decrease over the gyre, which is four times larger, corresponds to a similar freshwater addition in its upper 100 m. The total would be equivalent to an increase of ~50 km³ a^{-1} in the melt rate of continental ice. That volume is negligible in relation to interannual variability in ice sheet attrition, as attested by the recent major calving events, but it is a large change to be sustained over four decades, given an annual ice sheet budget of ~2000 km³ a^{-1} (14). We noted above that lower salinity (density) should reduce the strength of circulation and melting in the cavity beneath the Ross Ice Shelf, much of which is also buffered by source waters at or near the sea surface freezing point (Fig. 2). CDW intrusions beneath floating glacial ice in

the southeast Pacific are ~2°C warmer than MCDW in the Ross Sea, however, and are known to drive local melt rates two orders of magnitude higher (14).

CDW is characterized by a temperature maximum (T_{max}) at depths of ~200 to 400 m in the Ross Gyre. The T_{max} has warmed over recent decades, particularly in the southern half of the gyre (Fig. 3C), and has shoaled by ~50 m over the same period. That shoaling suggests the gyre circulation has not weakened, which could otherwise have slowed the upwelling of saltier water, contributing to the observed salinity decrease. The warming is similar to that documented for the upper 300 m of the global ocean during the late 20th century and to a recent deep water temperature increase in the Weddell Sea (19, 20). Where the CDW has access to southeast Pacific ice shelves, basal melting is likely to have increased (21). Ice shelves have recently

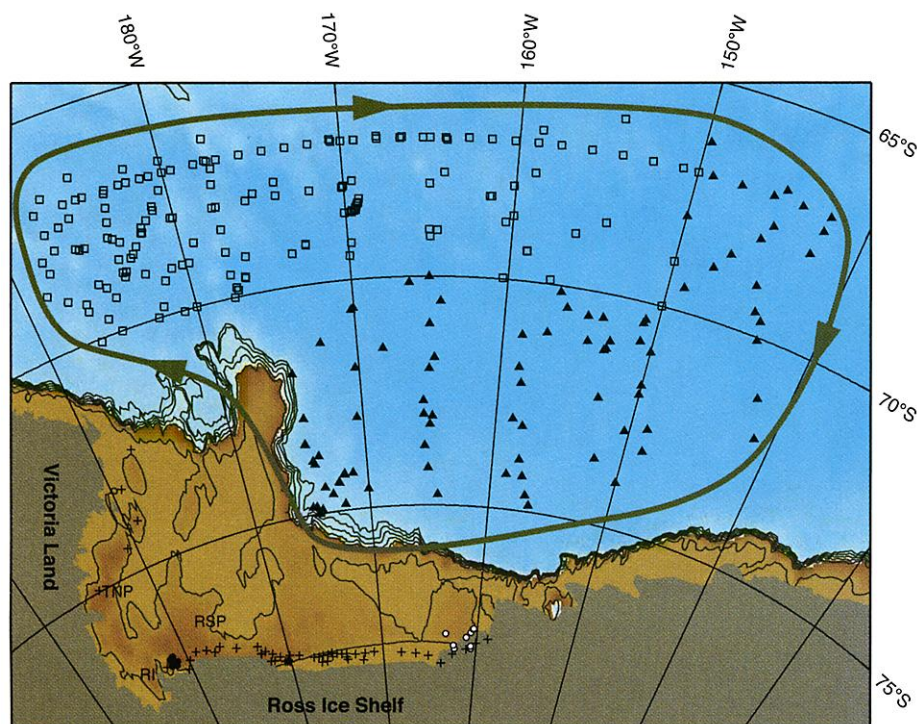


Fig. 1. Locations of ocean stations studied, and of the Ross Sea and Terra Nova Bay Polynyas (RSP and TNP, respectively). The profiles in Fig. 2 were taken at the solid circles near Ross Island (RI). A subset of that data is compared with similar observations near the eastern end of the Ross Ice Shelf front (open circles) in Fig. 3A. Stations within the Ross Gyre, north of the continental shelf (brown), were divided into seven roughly equal areas (not shown) to assess regional variability, with larger differences appearing between the northwest (open squares) and southeast (solid triangles) sectors (Fig. 3, B and C). Bathymetric contours (ETOPO5) are at 500 m and each 250 m from 1000 to 2000 m. Crosses indicate the positions of oxygen isotope and salinity measurements shown in Fig. 4.

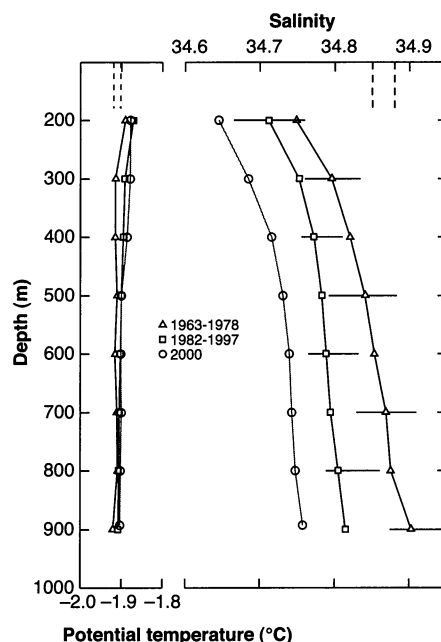


Fig. 2. Summer temperature and salinity profiles below 200 m near the western end of the Ross Ice Shelf (Fig. 1). The 1963-to-1978 profile is an average of measurements from five stations from 20 December to 6 February, whereas the 1982-to-1997 profile is an average from six stations taken from 8 December to 9 February. The most recent recording was on 15 February 2000. Horizontal bars indicate the variability within each aggregate salinity profile. The vertical dotted lines at top right show the salinity range that could result from winter variability of 18% in surface wind and 2 to 3°C in air temperature over a 4-year period (4). That band is 2 to 3 times wider than the accuracy of historical salinity measurements. Dashed lines at top left show the surface freezing temperatures spanned by the observed salinities. The open continental shelf is relatively deep at this location, but an average depth of 750 m roughly accounts for water that circulates in the sub-ice shelf cavity.

been thinning in the Amundsen Sea, and deflation of continental ice has occurred in the Pine Island and Thwaites drainage basins

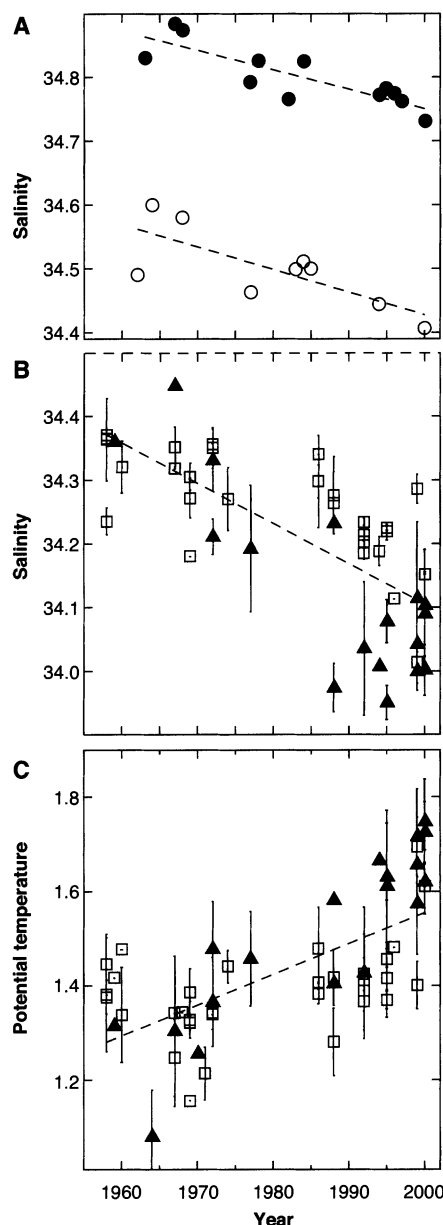


Fig. 3. (A) Salinity at 500 m (from Fig. 2) near the western (solid circles) and eastern (open circles) ends of the Ross Ice Shelf front, with corresponding regressions of -0.0030 [a correlation coefficient (r^2) equal to 0.85] and -0.0035 ($r^2 = 0.76$). A similar decline has been documented from data available through 1995 (6) for the shelf region west of 180° . (B) Salinity at the 25- to 130-m depth T_{min} in the Ross Gyre, with a regression of -0.0063 a^{-1} ($r^2 = 0.72$). The solid triangles and open squares with $\pm 1 \sigma$ correspond to annual averages in seven gyre subregions within the southeast and northwest sectors, respectively, of Fig. 1. (C) Temperature at the 190- to 440-m depth of T_{max} in the Ross Gyre. As in (B), the regression ($+0.0065 \text{ a}^{-1}$; $r^2 = 0.66$) is calculated from subregional annual means. Symbols are as in (B) and show larger changes in the southeast than in the northwest sector of the gyre.

(22, 23). These measurements are compatible with the increased availability of meltwater from that part of the West Antarctic Ice Sheet.

Seawater oxygen isotope measurements are also consistent with increased meltwater in the Ross Sea. All water masses have shifted toward lighter (more $\delta^{18}\text{O}$ -depleted) values in the 16 or 22 years between repeated observations on the continental shelf (Fig. 4). Ice shelf water (ISW) has changed the least, consistent with a longer residence time and little if any increased melting under the Ross Ice Shelf. Its salinity increase in 1994 resulted from fewer shallow measurements that year. From 1978 to 1994, the Antarctic Surface Water (AASW) and a weighted mean of all values slope toward $\delta^{18}\text{O}$ values of -29.1 and -39.4 per mil (‰), respectively, at zero salinity. For the period 1978 to 2000, the $\delta^{18}\text{O}$ value of the AASW at zero salinity is -17.0 ‰ and the weighted mean of all $\delta^{18}\text{O}$ values projects to -34.7 ‰. Because the $\delta^{18}\text{O}$ in snow ranges from -10 to -20 ‰ directly seaward of the West Antarctic coastline (24), the 2000 data set suggests recent precipitation in the AASW. However, the more negative projections of the other extrapolations indicate the presence of melted continental ice (16, 21).

Any one of these processes does not readily account for the magnitude of the salinity decline in the Ross Sea. Freshening may be relatively strong in the Ross Sea because of its teleconnection to the tropical Pacific (25), in combination with an altered Southern Oscillation pattern since the 1970s (26). But for

the freshening to have resulted mainly from a change in precipitation would have required that poleward moisture transport in the atmosphere be much larger than modeled or observed at higher latitudes on the ice sheet. If coupled with stronger winds, however, a "spinup" of the polar gyre circulation could cause sea ice divergence and shoaling of the T_{max} . Fresher surface water would increase the strength of the pycnocline (vertical density gradient), retaining heat in the deep water (27). If more or warmer deep water then intruded onto the Antarctic continental shelf, particularly in the southeast Pacific (14), increased basal melting of ice shelves could be expected (28). Most of the coastal flow in that sector is westward, toward the southern limb of the Ross Gyre, where we see the strongest salinity change. Reduced vertical heat flux from the deep water would also allow an increase in sea ice extent, as observed over the 1979 to 1998 period. This is consistent with a lower ice and brine volume production in strong source regions like the southwest Ross Sea, where air temperatures have risen since 1957.

The decreased salinity of the Ross Sea will have contributed to the reported freshening of intermediate waters originating in the Southern Ocean. It will have altered the characteristics if not the volume of locally produced deep and bottom waters, changes that have been observed downstream (29). Synoptic treatment of salinity observations that showed negative offsets between early and recent measurements (30) would now appear to represent real temporal change. A freshen-

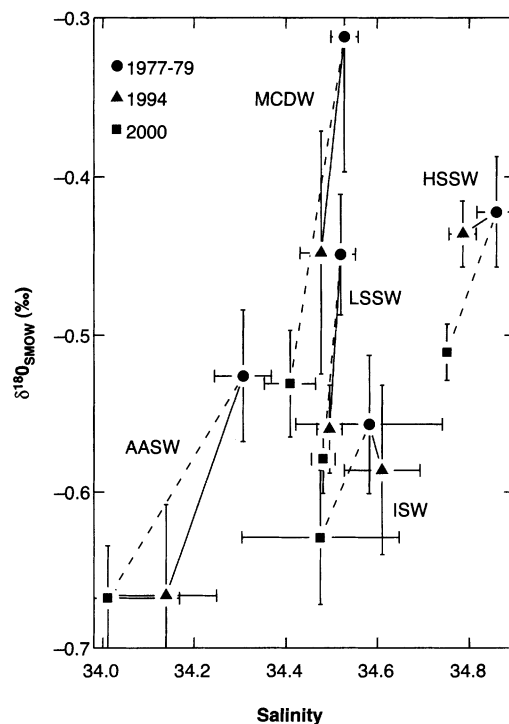


Fig. 4. Oxygen isotope and salinity relations for seawater in the southern Ross Sea (Fig. 1) aggregated by water mass characteristics and date of sampling. AASW, MCDW, low salinity shelf water (LSSW), ISW, and high salinity shelf water (HSSW) are represented by the means ($\pm 1 \sigma$) of 4 to 32 (an average of 11) values, all from duplicate determinations of up to four samples per water mass on each station. Individual oxygen isotope samples were processed at Lamont to a precision of ~ 0.025 ‰ as compared to standard mean ocean water (SMOW) (16). Salinities were analyzed aboard the ships or taken from corrected conductivity-temperature-depth profiles, accurate to within 0.01‰. A mean of all samples weighted by water mass area on a transect along the Ross Ice Shelf front shifted by -0.063 in salinity and -0.071 in $\delta^{18}\text{O}$ over the 16 years ending in 1994, and a weighted mean over 22 years ending in 2000 shifted by -0.120 in salinity and -0.119 in $\delta^{18}\text{O}$.

ing that exceeds the likely precipitation and sea ice changes and carries a low $\delta^{18}\text{O}$ signal also suggests an acceleration in the melting rate of West Antarctic ice shelves east of the Ross Sea.

References and Notes

1. S. Manabe, R. J. Stouffer, M. J. Spelman, K. Bryan, *J. Clim.* **4**, 785 (1991).
2. P. Huybrechts, J. DeWolde, *J. Clim.* **12**, 2169 (1999).
3. A. P. S. Wong, N. L. Bindoff, J. A. Church, *Nature* **400**, 440 (1999).
4. D. Bromwich, Z. Liu, A. N. Rogers, M. L. Van Woert, *Antarct. Res. Ser.* **75**, 101 (1998).
5. M. L. Van Woert, *J. Geophys. Res.* **104**, 7753 (1999).
6. S. S. Jacobs, C. F. Giulivi, *Antarct. Res. Ser.* **75**, 135 (1998).
7. G. Birnbaum *et al.*, in *Reports on Polar and Marine Research* (Alfred-Wegener Institute, Bremerhaven, Germany, 2001), vol. 380, pp. 64–92.
8. K. Grosfeld *et al.*, *Antarct. Res. Ser.* **75**, 319 (1998).
9. M. O. Jeffries, U. Rudolphs, *Antarct. Sci.* **9**, 188 (1997).

10. Data available at <http://ingrid.ldeo.columbia.edu/SOURCES/NOAA/NCAP-NCAR/CDAS-1/MONTHLY/>
11. H. J. Zwally, J. C. Comiso, C. L. Parkinson, D. J. Cavalieri, P. Gloersen, *J. Geophys. Res.*, **107**, 9–1 (2002).
12. C. L. Parkinson, *Ann. Glaciol.* **34**, 435 (2002).
13. S. S. Jacobs, J. C. Comiso, *J. Clim.* **10**, 697 (1997).
14. S. S. Jacobs, H. H. Hellmer, A. Jenkins, *Geophys. Res. Lett.* **23**, 957 (1996).
15. H. H. Hellmer, S. S. Jacobs, *J. Geophys. Res.* **100**, 10873 (1995).
16. S. S. Jacobs, R. G. Fairbanks, Y. Horibe, *Antarct. Res. Ser.* **43**, 59 (1985).
17. R. I. Cullather, D. H. Bromwich, M. L. Van Woert, *J. Clim.* **11**, 334 (1998).
18. R. Kwok, J. C. Comiso, *J. Clim.* **15**, 487 (2002).
19. S. Levitus, J. I. Antonov, T. P. Boyer, C. Stephens, *Science* **287**, 2225 (2000).
20. R. Robertson, M. Visbeck, A. L. Gordon, E. Fahrbach, *Deep-Sea Res.*, in press.
21. H. H. Hellmer, S. S. Jacobs, A. Jenkins, *Antarct. Res. Ser.* **75**, 83 (1998).
22. A. Shepherd, D. J. Wingham, J. A. D. Mansley, *EOS* **82**, F537 (2001).

23. A. Shepherd, D. J. Wingham, J. A. D. Mansley, H. F. J. Corr, *Science* **291**, 862 (2001).
24. M. O. Jeffries, A. L. Veazy, K. Morris, H. R. Krouse, *Ann. Glaciol.* **20**, 33 (1994).
25. X. Yuan, D. Martinson, *J. Clim.* **13**, 1697 (2000).
26. D. M. Karl *et al.*, *Oceanography* **14**, 16 (2001).
27. A. Gordon, *Proceedings of the Carbon Dioxide Research Conference: CO₂, Science and Consensus*, 19 to 23 September 1982, Berkeley Springs, WV (Institute for Energy Analysis, Washington DC, 1983), pp. IV.76–IV.86.
28. E. Rignot, S. S. Jacobs, *Science* **296**, 2020 (2002).
29. T. Whitworth, *Geophys. Res. Lett.* **29**, 17 (2002).
30. V. V. Gouretski, K. A. Janke, *J. Atmos. Ocean. Technol.* **16**, 1791 (1999).
31. Supported by the NSF and NASA Polar Programs, with assistance from NOAA for oxygen isotope analyses by R. Mortlock. We thank A. Klepikov for 1988 Russian data, the New Zealand National Institute of Water and Atmospheric Research for Scott Base temperatures, and three readers who provided helpful comments.

7 January 2002; accepted 4 June 2002

The Function of the Cranial Crest and Jaws of a Unique Pterosaur from the Early Cretaceous of Brazil

Alexander W. A. Kellner^{1*†} and Diogenes de Almeida Campos^{2*}

The discovery of a previously undescribed pterosaur, *Thalassodromeus sethi*, yields information on the function of cranial crests and the feeding strategy developed by these extinct flying reptiles. The material consists of a large skull (length: 1420 millimeters, including the crest) with a huge bony crest that was well irrigated by blood vessels and may have been used for regulation of its body temperature. The rostrum consists of two bladelike laminae, the arrangement of which is analogous to the condition found in the bird *Rynchops*, which skims over the water to catch food, indicating that *T. sethi* also may have been a skimmer.

Despite being studied for over 200 years, the overall knowledge of pterosaur diversity and biology is rather slim, mainly due to uneven sampling and the generally poor preservation of specimens (1, 2). Moreover, because pterosaurs are extinct, their biological habits and functions of anatomical features are difficult to establish, and most interpretations have relied on comparisons with modern analogs such as birds. Here, we report a previously undescribed pterosaur that shows a distinct morphology of the skull, providing information on the function of cranial crests and feeding strategy. The specimen comes from

the Romualdo Member of the Santana Formation (3), in the Araripe Basin, in northeastern Brazil, which is one of the few deposits where pterosaurs are found in large numbers with good preservation.

The sedimentary rocks of the Santana Formation were deposited during the Early Cretaceous (Aptian/Albian) and represent two distinct *lagerstätten*, formed by the lacustrine limestone layers of the Crato Member at the base and the lagoonal limestone concretions embedded in shales of the Romualdo Member at the top (4, 5). Although pterosaurs have been found in the lower layers (2, 6–8), the deposits in the Romualdo Member contain better-preserved specimens (9–12). The material described here was preserved in a calcareous nodule from this deposit and consists of an almost complete skull (Fig. 1), representing a new species.

Pterosauria Kaup, 1834
 Pterodactyloidea Plieninger, 1901
 Tapejaridae Kellner, 1989
Thalassodromeus nov. gen.
T. sethi nov. sp.

Etiymology: Thalassodromeus from the

Greek *thálassa* (= sea) + *dromeús* (runner) meaning the “sea runner”; *sethi* for the ancient Egyptian god Seth.

Holotype: skull (total length, 1420 mm; length from the squamosal to the tip of the premaxilla, 798 mm) and lower jaw (length: preserved, 635 mm; estimated, 710 mm) deposited at the Museu de Ciências da Terra/Departamento Nacional de Produção Mineral (DGM 1476-R) (Figs. 1 to 3); cast at the Museu Nacional (MN)/Universidade Federal do Rio de Janeiro (UFRJ) (MN 6678-V).

Horizon and locality: The specimen was collected in 1983 at the outcrops of the Romualdo Member [Albian (3, 5)], in the Santana Formation, near the town of Santana do Cariri, in the state of Ceará, northeastern Brazil.

Diagnosis: Tapejarid with developed cranial crest composed of premaxillae, frontal, parietal, and supraoccipital, starting at the tip of the skull and extended posteriorly, well behind the occipital region; posterior end of the cranial crest V-shaped; suture between premaxillae and frontoparietal portion of the crest rectilinear; anterior portion of the premaxillae and dentary with sharp dorsal and ventral edges; palatines before palatal crest strongly concave; posterior (occipital) region broader than in other tapejarids (width over quadrates, 20% of squamosal to premaxilla length).

With the exception of two segments from the ventral part of the skull plus the mandible and the distal tip of the lower jaw, the material is complete and all bones are preserved in three dimensions. The only signs of compaction are found in the region of the left jugal and in the right mandibular ramus, which are slightly pushed inward.

As is typical of derived pterosaurs (members of the clade Pterodactyloidea), *T. sethi* has an elongated skull (Fig. 1). The orbit is positioned lower than the dorsal rim of the antorbital fenestra, a feature only present in the azhdarchids [e.g., *Quetzalcoatlus* sp.

¹Paleovertebrate Sector, Department of Geology and Paleontology, Museu Nacional/Universidade Federal do Rio de Janeiro, Quinta da Boa Vista, São Cristóvão, Rio de Janeiro, RJ, 20940–040, Brazil. ²Museu de Ciências da Terra/Departamento Nacional de Produção Mineral, avenida Pasteur 404, Rio de Janeiro, RJ, 22290–240, Brazil.

*The authors are fellows at Conselho Nacional de Desenvolvimento Científico e Tecnológico and associate researchers at the American Museum of Natural History.

†To whom correspondence should be addressed. E-mail: kellner@mn.ufrj.br